Model-Based Exhaust Gas Temperature Control to Reduce the Mixture Enrichment at High Loads

20XX-01-XXXX

Model-Based Exhaust Gas Temperature Control to Reduce the Mixture Enrichment at High Loads

Author, co-author (Do NOT enter this information. It will be pulled from participant tab in MyTechZone)

Affiliation (Do NOT enter this information. It will be pulled from participant tab in MyTechZone)

Abstract

In this work an exhaust gas temperature and a piston damage model are coupled, with the aim to develop an innovative, model-based strategy for the calibration of the lambda map and to actively control the spark advance. In this way, the lambda value needed to reach a target exhaust gas temperature evaluated at the turbine inlet is determined. In the first part of the paper, some empirical and semi-physical models for the calculation of the exhaust gas temperature, the combustion phase, the maximum in-cylinder pressure and the knock intensity are developed and presented. A piston damage model previously developed by the authors determines the spark advance to reach a target piston erosion for the knock-limited operating conditions, increasing the combustion efficiency and lowering the temperature of the exhaust gases with respect to the standard spark timing map. The exhaust gas temperature model allows to estimate the lambda value that returns the maximum temperature at the turbine inlet, exploiting the gained combustion efficiency to extend the stoichiometric area of the engine operating field.

In the last part of the work, the lambda map calibrated through the proposed algorithm is validated for both the transient and steady-state conditions, reproducing a real vehicle maneuver at the engine test bench. The results finally demonstrate that a combustion efficiency increase equal to 8% can be reached by managing the spark advance with a piston damage-based controller and this number can be increased up to 16 % applying the recalibrated lambda map, with respect to the standard engine calibration.

Keywords: combustion, knock, efficiency, modelling, control, exhaust, temperature, turbine, spark advance, lambda

Introduction

During the past years, the increasingly stringent, anti-pollution and anti-CO_2 regulations forced the manufactures to increase the efficiency of internal combustion engines. The main technical solutions exploited during the last decade to increase the specific power and the efficiency of the Spark Ignition (SI) engines, are both the downsizing and the application of the turbocharger. However, these solutions also lead to increase the engine knock tendency, especially under high load operating conditions. This is due to higher pressure and temperature of the mixture inside the combustion chamber with respect to a naturally aspirated engine. The commonly adopted strategy to avoid the damage of the combustion chamber components induced by knocking events is the Spark Advance (SA) and the combustion phase retarding, that reduces the combustion efficiency [1] and increases the exhaust gas temperature. Typically, it is thus necessary to enrich the mixture to reduce such temperature [2] and to avoid damages to the turbine impeller [3]. It can be stated that the abnormal combustions and the high exhaust gas temperatures represent the main limits to the benefits brought by the application of the downsizing and turbocharging technologies.

These phenomena are still an issue for the engine designers and the control developers, despite the application of innovative solutions thought to reduce their impact in the modern GDI Turbo-Charged (TC) engines (such as the low-pressure exhaust gas recirculation [4], the port or direct water injection [5] and the pre-chamber systems [6]). This is also because the knock intensity thresholds and the criteria applied to the SA calibration process are typically the result of the manufacturer experience and, in most cases, are defined to avoid the knocking combustions at all. The highest percentiles (such as the 98th or the 99th) or even the cyclic intensity values are controlled to avoid the complete exceedance of some sort of experience-driven limit. Moreover, such thresholds have remained the same over the years, not following the improvements in the materials strength [7]. The updates in the alloy mechanical characteristics led to a significant increase of the admissible maximum pressure inside the combustion chamber, not necessarily followed by a corresponding redefinition of knock intensity thresholds. This is certainly due to an increase of the thermal and mechanical load on the combustion chamber components, that affects the alloy resistance, but also the lack of a robust, quantitative relationship between the calculated knock index, and the corresponding induced damage.

As well known, the SA and the target lambda value are the two main parameters that have to be optimized in order to maximize the combustion efficiency. The development of robust, empirical knock intensity and exhaust gas temperature models is based on the estimation of other relevant combustion indexes, such as the combustion phase and the maximum in-cylinder pressure. Different approaches can be found in literature to calculate the combustion phase, depending on the final application. The most suitable approach for the Real-Time (RT) or the control-oriented codes is the analytical one [8]. More physical methodologies, based on predictive combustion models, are also implemented for Software-in-the-Loop and RT simulations [9,10]. More recently, even the machine learning-based algorithms and the neural networks are implemented for the combustion phase estimation [11].

As mentioned above, together with knock, the exhaust gas temperature has a key role in the management of the maximum conversion efficiency of the aftertreatment system. Differently from the installation at the engine test bench, the thermocouples or other similar sensors are not used on the final on-board application for reliability and cost reasons. Indeed, the exhaust gas temperature is often estimated through dedicated models that are implemented in the Engine Control Unit (ECU) code [12]. More recently, some machine learning-based algorithms have been developed to estimate such temperature even under dynamic conditions [13, 14].

The main methodologies for the knock intensity calculation are both the 1-D and 0-D modelling and several approaches can be found in literature [15-22]. Most of them assume that the mixture within the combustion chamber is separated in two different zones, that contain the burned and unburned gases [15-19], respectively. The pressure, the temperature and the composition of the unburned zone are calculated through the chemical kinetics [15, 16] to predict the autoignition event. Nevertheless, the algorithms that use the mentioned approaches are not suitable for the multicycle simulations [17]. Alternatively, the abnormal combustion occurrence is calculated through the integral approach proposed by Livengood and Wu in [18]. This method is based on the calculation of the ignition delay estimated by a multivariable equation expressed via the Arrhenius formula. The intensity of the instantaneous event is typically calculated by reproducing an index comparable with the experimental Maximum Amplitude of Pressure Oscillation (MAPO). A physical approach for the estimation of the abnormal combustion intensity considers the

instantaneous pressure increase generated by an isochoric combustion of the unburned mixture residual fraction [19, 20]. Even if such method is compatible with the RT execution [21], it cannot accurately describe the cyclic variation of the instantaneous intensity. For this reason, it is common estimating the statistical indexes of MAPO for fixed engine operating conditions. Indeed, as well known, its probability distribution can be accurately described with a Weibull, Gamma, or Log-normal Probability Density Function (PDF) [22, 23]. The latter is completely identified with only two parameters (the mean value and the standard deviation, or two properly chosen percentiles) as for the Gaussian PDF, from which it inherits even the main properties. Such feature allows to calculate the knock intensity with a pure analytical approach [24]. The main parameters needed to describe the MAPO log-normal PDF for given engine operating conditions are the 50th and the 98th percentiles. Indeed, such values are directly related to the mean value and the standard deviation of the statistical distribution.

In this work, a novel, model-based algorithm to automatically calibrate the lambda map is presented. The resulting function is mainly composed by a piston damage model and a turbine inlet gas temperature model. The first determines the spark advance to reach a target piston erosion for the knock-limited operating conditions, increasing the combustion efficiency and lowering the temperature of the exhaust gases, while the latter allows to exploit the gained efficiency to extend the stoichiometric portion of the engine operating field.

In the first part of this paper, a reliable and accurate control-oriented engine simulator is developed and validated. With such virtual engine it is possible to calculate the main combustion indexes, such as the Crank Angle that corresponds to the 50 % of the Mass of Fuel Burnt (CA50), the maximum in-cylinder pressure (PMAX), the exhaust gas temperature at the turbine inlet and the MAPO, which is the index used in this work to estimate the knock intensity. A Wiebe-based combustion model is calibrated to reproduce the in-cylinder pressure trace for each engine operating condition, as described in a previous work by the authors [25]. With this model the Temperature at Exhaust Valve Opening (TEVO) and the CA50 are calculated. An Artificial Neural Network-based (ANN) model is instead developed to calculate the knock intensity, for fixed engine operating conditions and PMAX, the engine load, speed, lambda, and the intake manifold air temperature are used as inputs for such model. A Feedforward Neural Network (FNN) is implemented in the algorithm for the knock intensity estimation. The maximum in-cylinder pressure is defined through an analytical equation, using the engine load and the CA50 as independent variables [26].

The offline calibration of the lambda map is carried out by evaluating the Knock-Limited Spark Advance (KLSA) value for each engine operating condition. One of the most common ways to define the KLSA is to determine the SA for which the 1% of a certain number of cycles is characterized by a MAPO value higher than a given threshold [27], usually determined by the experience of the engine manufacturer. This criterion is also implemented in the majority of the combustion control systems [28], but it is an extremely safe approach thought to avoid damages to combustion chamber components at all. In this work, a control-oriented piston damage model developed and validated in previous works by the authors [29-31] is implemented to convert MAPO into a more tangible and concrete intensity index and for targeting the admissible damage generated by knocking combustions on the piston surface in a certain amount of time (i.e., the target damage speed). The calculation of such quantity is based on a threshold (empirically calibrated as a function of the modelled piston temperature) that distinguish between MAPO values which produce or not the piston surface erosion. Such threshold has been defined by performing metallurgical analysis on numerous damaged pistons. With such approach, it is possible to define the KLSA getting the admissible piston surface erosion and increasing the combustion efficiency.

Through the implementation of all the mentioned models, the KLSA and the lambda value that allows to achieve the maximum exhaust gas temperature at the turbine inlet can be determined. In this way, the overall efficiency of the energy conversion process is increased (the specific fuel consumption is decreased) and, at the same time, the combustion chamber components, and the turbine impeller integrity is preserved.

In the last part of the paper, the results of the experimental tests carried out to validate the proposed calibration procedure are finally presented. Both the model-based SA controller coupled with the lambda map calibrated with the proposed algorithm are validated reproducing a real vehicle maneuver at the engine test bench and thus testing both the transient and steady-state conditions. Such tests allow to achieve an overall efficiency increase equal to 16%.

Experimental Setup

The experimental tests are carried out on a V8, 3.9 liters, GDI, TC engine equipped with a piezoelectric sensor for each cylinder and a thermocouple is mounted at the turbine inlet of each engine bank. Further features of such engine are reported in Table 1.

Table 1. Engine characteristics.

Displaced volume	3.9 L (8 cylinder) - turbo
Stroke	82 mm
Bore	86.5 mm
Connecting Rod	143 mm
Compression ratio	9.45:1
Number of Valves per Cylinder	4

The experimental tests are performed covering a wide part of the engine operating range, investigating especially the area characterized by the highest engine load and speed. Figure 1 shows the engine points tested during the experimental campaign. The engine load is defined as the volumetric efficiency and all the main variables are normalized with respect to the maximum value of each figure for confidentiality reasons.

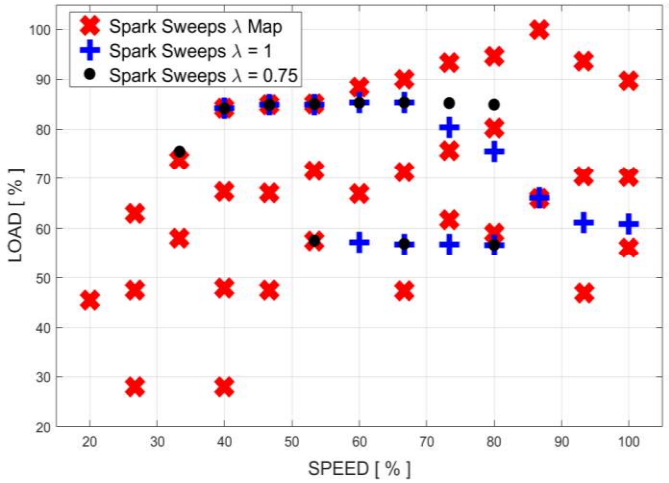

Figure 1. Engine operating conditions for which experimental tests are carried out at different lambda values.

For each steady-state condition, the SA is changed performing a spark sweep. Some tests are repeated with different lambda values, providing the experimental data needed to calibrate the influence of the mixture quality on the main combustion indexes. The tested steady-state conditions (keeping constant the engine speed, load, SA, and lambda) are about 700. However, such database comes from an engine characterization experimental campaign, collected to calibrate the ECU control strategies. In other words, such kind of combustion data have not been logged for this specific modelling activity but are typically always available. The in-cylinder pressure signals are recorded for 200 consecutive cycles with a sampling frequency of 200 kHz, using the Alma Automotive mASTRO charge amplifier and OBI

as indicating system (provided by the same manufacturer). The combustion phase, its duration and the PMAX are estimated from the low-pass-filtered pressure curves, with a cut-off frequency of 3 kHz. MAPO is used as the knock intensity index, and it is determined with the Equation 1:

$$MAPO = \max\left(abs\left(p_{filt}\right)\right) \quad (1)$$

Where p_{filt} is the band-pass filtered in-cylinder pressure signal and the cut-off frequencies are not disclosed for confidentiality reasons. The same value of the recorded cycles (200) has been previously used for the development and validation of other models and, for this reason, it represents the reference for the evaluation of the combustion and knock indexes even in this work. Moreover, the record is typically started after the steady-state condition is reached, and, in this way, also the measurement of the thermocouples can be considered reliable and accurate. The algorithms described in this work are developed for the mean cylinder and the mean values of the 98th and the 50th percentiles of MAPO (named MAPO98 and MAPO50 in the following sections of the paper, respectively) are considered to characterize the knock intensity of a certain operating condition. Finally, the exhaust gas temperature is measured with a thermocouple installed at the turbine inlet of each engine bank and directly exposed to the exhaust gases. Even in this case, the thermocouple measurements for the two engine banks are averaged. The main features of the mounted thermocouples are reported in Table 2.

Table 2. Thermocouple characteristics.

Type	K
Diameter	3 mm
Accuracy	± 2.2 C°

The device used to log the thermocouple signal is a National Instruments Compact-RIO 9024, on which the specific module 9213 is installed. The signal is recorded with a sampling frequency of 100 Hz. Such frequency is enough to characterize the exhaust gas temperature for a given engine point, because the measurements are performed under steady-state conditions.

Combustion Model

The virtual engine is composed by four models, thought to accurately reproduce the combustion phase, the maximum in-cylinder pressure, the knock intensity, and the exhaust gas temperature.
A 0-D combustion model based on the Wiebe equation has been previously developed by the authors in [8]. Once the main parameters D (that represents the combustion duration) and E (the Wiebe exponent) are calibrated, it is possible to simulate with high accuracy the average pressure curve in the closed-valve portion of the engine cycle (the range -60 - +140 CA° is chosen). Further details about the algorithm implemented for the model calibration are described in [8]. For the sake of clarity, only the main equations included in such algorithm are reported below:

$$dT = \frac{dQ_{comb} - dQ_{wall} - pdV}{c_v M} \quad (2)$$

$$dQ_{comb} = \lambda m_{fuel} LHV \frac{d\chi(\vartheta)}{d\vartheta} \quad (3)$$

$$\chi\left(\vartheta\right) = 1 - \exp\left(-WC\ \left(\vartheta - SOC\right)^{E+1}\right) \quad (4)$$

$$WC = \left(\frac{D}{BEC^{\frac{1}{E+1}} - BSC^{\frac{1}{E+1}}}\right)^{-(E+1)} \quad (5)$$

$$BEC = -\ln(0.1) \quad (6)$$

$$BSC = -\ln(0.9) \quad (7)$$

$$fo = \sum_{i=1}^{n} \frac{\left|p_{exp}(i) - p_{sim}(i)\right|}{n} \quad (8)$$

Where:

- dT is the infinitesimal gas temperature variation. Of course, the initial conditions are needed to properly solve the Equation (2). As described in [8], a polynomial function with the engine load and speed as independent variables has been developed to calculate the in-cylinder pressure value at the start of the closed-valve portion of the cycle (i.e., -60 CA°). For a certain mixture mass inside the combustion chamber, the pressure value is converted into the corresponding temperature with the perfect gas law
- dQ_{comb} represents the infinitesimal energy provided by the combustion of the stoichiometric mixture ($\lambda m_{fuel} LHV$), described through the Wiebe function $\chi\left(\vartheta\right)$. The main calibratable parameters of such function are D and E included in the Wiebe Constant (WC). The other parameters needed to calculate WC are the Burned End Constant (BEC), the Burned Start Constant (BSC) and the Start of Combustion (SOC)
- dQ_{wall} is the infinitesimal energy loss towards the walls of the combustion chamber modelled with the Woschni formula
- dV is the infinitesimal variation of the volume
- p is the calculated pressure obtained by coupling the integral of Equation (2) with the perfect gas law
- c_v is the specific heat estimated considering the gas within the combustion chamber as a mixture of oxygen, nitrogen, vaporized fuel, carbon dioxide and water vapor [32]
- M is the trapped mass, which can be modelled with a polynomial function with the engine speed and load as inputs [8]. The values are calculated from the measured fuel consumption and lambda

The optimization algorithm finds the Wiebe parameters D and E for each operating condition by setting the SOC equal to the SA and minimizing the value of the objective function expressed by the Equation (8). In such equation p_{exp} is the experimental in-cylinder pressure trace, p_{sim} is the simulated one and n is the number of samples.

CA50 Model

A control-oriented CA50 model can be developed with the calibrated Wiebe parameters by reversing the following equation:

$$SOC = CA50 - \frac{D\ BMC^{\frac{1}{E+1}}}{BEC^{\frac{1}{E+1}} - BSC^{\frac{1}{E+1}}} \quad (9)$$

Where $BMC = -\ln(0.5)$. In the Equation (9), the acronym BMC means Burned Mean Constant. Since the 0-D combustion model is calibrated supposing the SOC coincides with the SA, the Equation (9) is modified as follows:

$$SA = CA50 - \frac{D\ BMC^{\frac{1}{E+1}}}{BEC^{\frac{1}{E+1}} - BSC^{\frac{1}{E+1}}} \quad (10)$$

As described in [8], the trend of the Wiebe parameters D and E is well defined with a polynomial function.
The novel contribution of this work is represented by the development of the lambda sensitivity for the CA50 model. A FNN-based method is applied for accurately including the four different independent inputs (i.e., the engine speed, load, SA, and lambda). The FNN is characterized by an analytical formulation that makes the calibration process particularly fast and the resulting function suitable for the RT execution on a development ECU. Moreover, some commercial applications for the data analysis provide integrated and user-friendly platforms (such as the Matlab Neural-Network fitting tool [33]) for the neural network automatic calibration. The structure of the FNN consists in a series of layers that are based on the product between a matrix (whose dimensions depend on both the number of inputs and neurons) and the array of the input variables. The result of such algebraic operation is added to a bias array and consequently an activation function calculates the output of the layer. The activation function is chosen between some standard functions such as the hyperbolic tangent sigmoid (tansig), log-sigmoid (logsig), radial basis (radbas) and radial basis normalized (radbasn) [33]. Figure 2 shows a scheme of a single layer FNN. The activation function of the final output layer is always a linear equation independently from the number of layers. The dimensions of the Matrix 2 depend on those of the Matrix 1 to make it compatible with the second product. This means that, for a fixed number of neurons of the first layer, the dimensions of the Matrix 2 and the bias 2 are automatically determined.

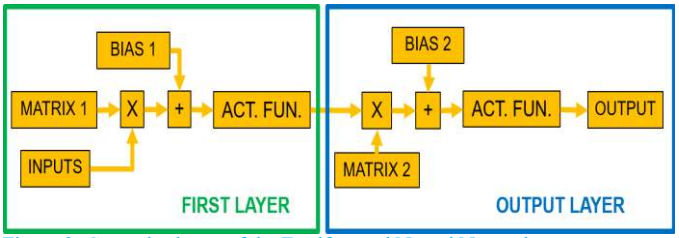

Figure 2. General scheme of the Feedforward Neural Network.

The CA50 model is based on two neural networks that use the SA, engine load, speed, and lambda as inputs to estimate the Wiebe parameters. The whole experimental database is divided into the training and the testing dataset, equal to the 75% and the 25% of the whole available database, respectively. The scaled conjugate gradient backpropagation training algorithm is used in this work for the network calibration [34]. The number of layers and the number of neurons for each layer are determined by the iterative loop shown in Figure 3. The main steps of such algorithm are summarized below:

1. Starting with 1 neuron, the neural networks layout is defined once the training algorithm, the number of layers, and the percentage of dataset used to train the network are determined
2. The neural networks are trained with the scaled conjugate gradient backpropagation algorithm
3. The trained neural networks calculate both the Wiebe parameters (*E* and *D*)
4. The CA50 is calculated by reversing the Equation (10)
5. The R-Square (R2) and the Root Mean Square Error (RMSE) indexes are calculated between experimental and simulated values of CA50 related to the testing dataset
6. The steps from 1 to 5 are repeated increasing the number of neurons until the maximum value, arbitrary chosen to reach the maximum accuracy of the network

Considering that the number of layers is equal to 1, the general structure of the two neural networks used to simulate the Wiebe coefficients is that reported in Figure 2. The activation function is the tansig, as discussed above.

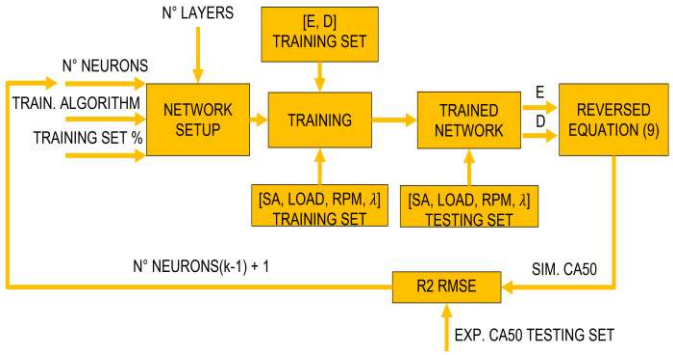

Figure 3. Iterative loop applied to calculate the value of neurons for the neural networks used to simulate the Wiebe function parameters.

The trends of R2 and RMSE that result from such calibration procedure are shown in Figure 4. The number of neurons is chosen as the lowest number that guarantees the highest value of the R2 and the lowest for the RMSE. The reported data are about the testing dataset.

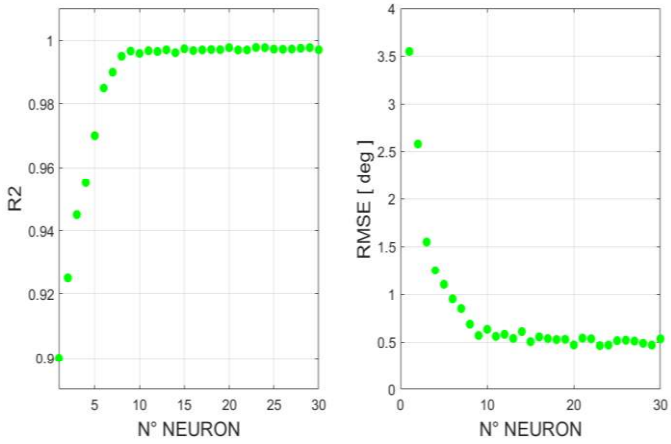

Figure 4. R2 and RMSE as a function of the number of neurons calculated between the simulated and the experimental CA50 for the testing dataset.

Considering the trends shown in Figure 4, it can be stated that using a number of neurons higher than 10 the overall accuracy does not increase. Moreover, such results demonstrate that a single layer is enough to have a reliable and accurate model. In Figure 5 the correlation between the experimental and the simulated CA50 values for the test dataset is shown. Since the RMSE is lower than 1 °CA, such result is a further demonstration of the model accuracy.

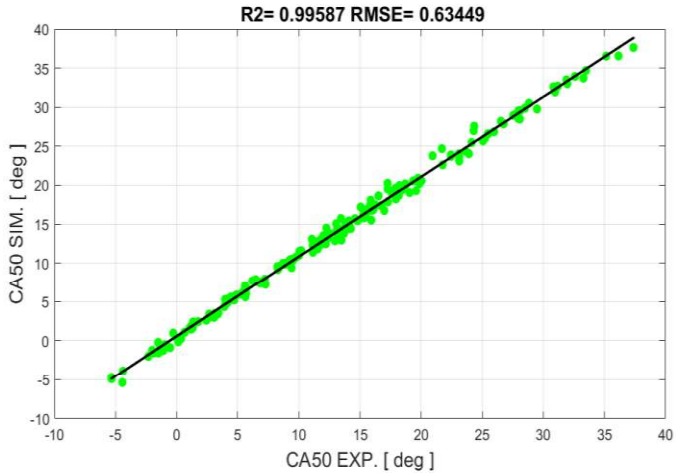

Figure 5. Correlation between the experimental and the simulated CA50 for the testing set, implementing the two calibrated neural networks for the calculation of Wiebe parameters *D* and *E*.

Knock Model

The Finite Element Method-based (FEM) piston damage model developed by the authors [31] allows to calculate the admissible damage speed for each engine operating conditions and consequently the related KLSA. The knock model is thus used to reproduce the intensity of instantaneous events. As introduced above, the log-normal PDF can well describe the MAPO statistical distribution [23, 24] for fixed operating conditions (engine speed, load, SA and lambda). This means that only two parameters are needed to completely define such kind of distribution (the mean value and the standard deviation). Indeed, the log-normal distribution benefits of the same properties of the Gaussian PDF and the mean value and the standard deviation can be determined once the 50th and another percentile are known. In this work, the 98th percentile is considered, and it is arbitrary chosen. With the following equations [25], the mean value and the standard deviation of the MAPO PDF are directly calculated from the mentioned percentiles:

$$\mu = \log(MAPO\ 50) \tag{11}$$

$$\sigma = \frac{\log(MAPO\ 98) - \mu}{2.0057} \tag{12}$$

Where μ is the mean value and σ is the standard deviation.
The MAPO98 can be estimated by modelling these two parameters and reversing the Equation (12). The development of the knock model is based on two FNNs used to estimate μ and σ, respectively. Based on the authors experience, PMAX is strongly related to knock intensity [25] and it can be used as one of the main inputs. In Figure 6 and 7 the trends of the standard deviation and the mean value are shown as a function of PMAX, for some spark sweeps performed at 5000 RPM. These tests are executed with the same engine load and with different conditions of lambda and intake air temperature, as reported in the legend of the two graphs. The lambda values are always between 0.75 and 1, and this is defined as the range in which even the values of the standard lambda map are included. The values reported in Figure 6 are the average between all the cylinders: this means that also the knock model will be developed for the mean one.

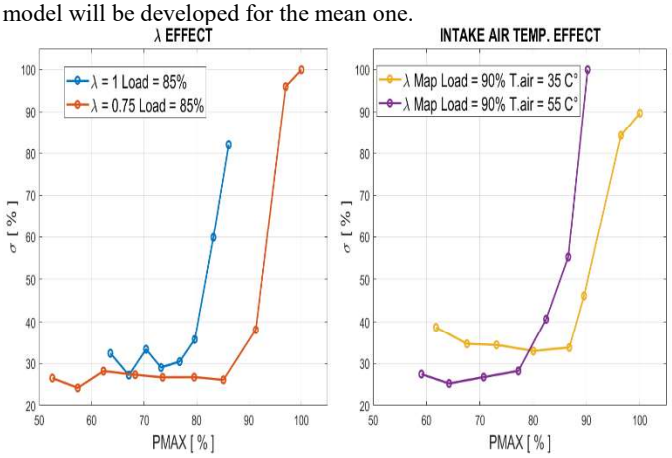

Figure 6. Trends of σ as a function of PMAX for different lambda values (left-hand plot) and for different intake air temperature (right-hand plot).

As shown in Figure 6, once a certain value of PMAX is reached, σ trend starts to increase rapidly under knock limited operating conditions. With this figure it is possible to highlight the importance of the lambda and the intake air temperature at the start of the engine cycle. The richer the mixture, the higher the PMAX for which the curve knee occurs. On the other hand, keeping constant the lambda and the engine load, it is possible to underline the effect of the intake air temperature on the knock intensity. Indeed, comparing the yellow and the violet trends reported in the right-hand graph of Figure 6, it is highlighted that the PMAX value that corresponds to the curve knee is reduced of 6-7%, while increasing the intake air temperature of 20 °C.

Figure 7 shows the trend of the mean value μ. While a different quality of the mixture has not a clear effect on the mean value of the MAPO PDF, the intake air temperature strongly affects such parameter. The higher the temperature, the higher the mean value of the statistical distribution.

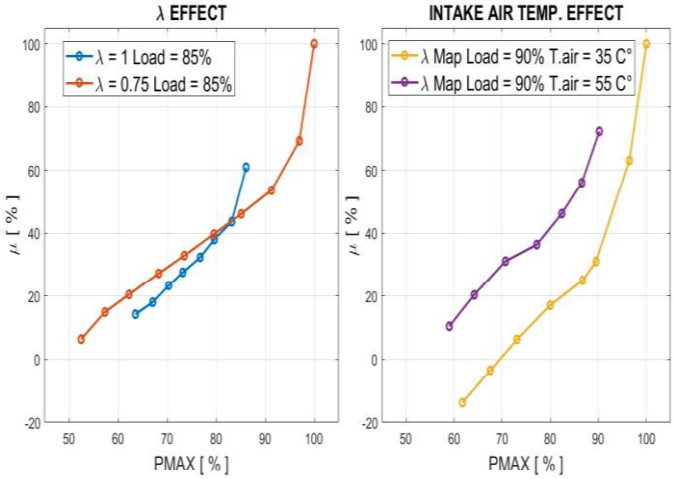

Figure 7. Trends of μ as a function of PMAX for different lambda values (left-hand plot) and for different intake air temperature (right-hand plot).

Such observations allow to state that the knock model needs the PMAX, lambda, the intake air temperature, the engine load, and speed as inputs. Of course, also the fuel quality (RON) influences the engine knock tendency [35]. Nevertheless, in this work such variable has not been considered, because all the experimental tests are carried out with the RON 95 fuel.
The procedure implemented to calibrate the number of neurons for the two neural networks developed to determine both μ and σ is that shown in Figure 4 and described above. Also in this case, a single layer neural network is implemented. Hence, the neurons number optimization is performed by comparing the experimental and the calculated MAPO98 for the test dataset. The R2 and RMSE indexes are calculated to quantify the model accuracy and the results are reported in Figure 8.

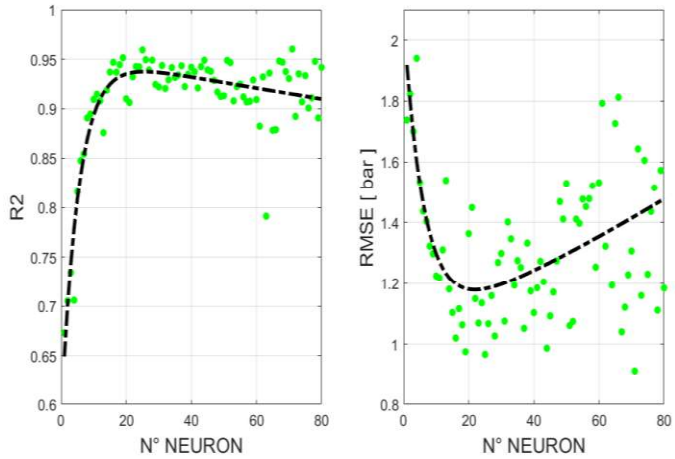

Figure 8. R2 and RMSE between simulated and experimental MAPO98 related to the test dataset as a function of the number of neurons.

This result can be compared with that reported in Figure 4 and it can be highlighted that in Figure 8 the green dots are more scattered around the dashed line. This aspect can be explained by analyzing the MAPO standard deviation exponential trend with respect to PMAX. Indeed, a small error of the μ model for high PMAX values (i.e., for high knocking conditions) can generate not negligible errors on MAPO98 due to the very steep slope of the μ curve after its knee. The weight of each NN on the calculation of MAPO98 can be evaluated with the following Figure 9, in which the same analysis of Figure 8 is reported for μ and σ.

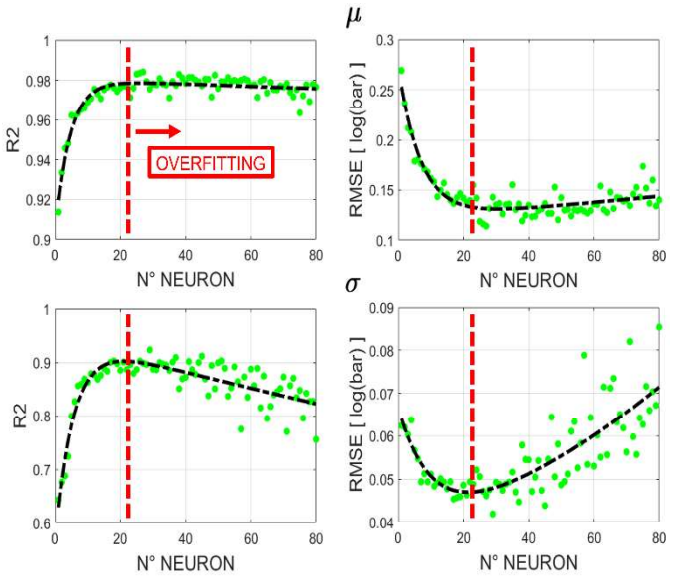

Figure 9. R2 and RMSE between simulated and experimental μ and σ related to the test dataset, as a function of the number of neurons.

The MAPO standard deviation model strongly affects the accuracy of the MAPO98 calculation and, therefore, such neural networks are more affected by the overfitting phenomenon, as highlighted in red in Figure 9.

It is analyzed the influence of the activation function on the accuracy of the proposed model. The iterative loop described above is repeated changing the activation functions for the first layer. In Figure 10 the fitted R2 trends are reported for all the tested functions.

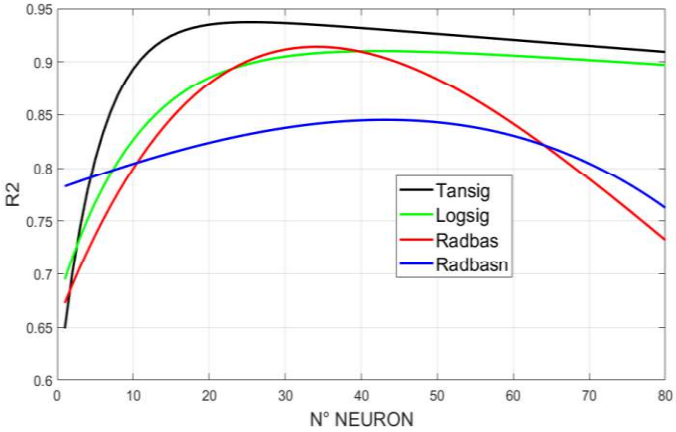

Figure 10. Fitted R2 trends for the comparison of the experimental and the simulated MAPO98 for different activation functions.

The analysis of Figure 10 demonstrates that the accuracy of the model calibrated with the tansig function and with a number of neurons between 20 and 30 is the configuration that ensures the highest accuracy. Hence, two 25 neurons, single layer FNNs with tansig activation function are implemented to estimate both μ and σ. In Figure 11 the performance of the resulting knock model is shown. The graph on the left shows the correlation between the experimental and the simulated MAPO98 for the testing dataset. The numerical data are reported as percentage values for confidentiality reasons, but the RMSE in the title of the left-hand plot is reported as physical unit (bar). The right-hand graph shows the experimental and the simulated MAPO distributions, referred to the operating condition at 4500 RPM and Wide-Open Throttle (WOT) included in the testing set. Such graph is zoomed to highlight the x-axis portion in which there is most of the recorded cycles, but the correlation reported on the left shows the values until the 100%. This is the engine point for which the maximum experimental MAPO98 is recorded.

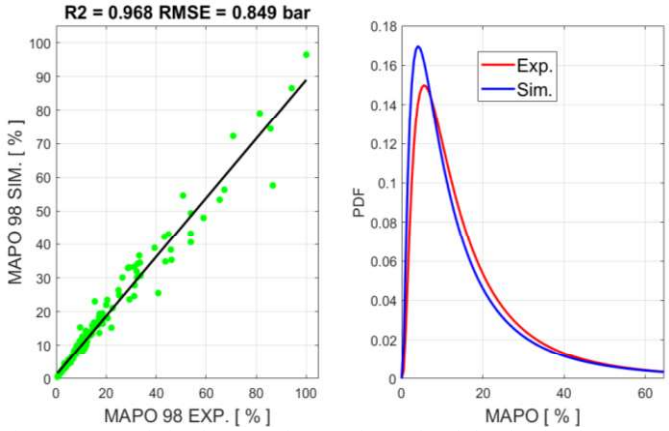

Figure 11. Correlation between the experimental and the simulated MAPO98 and log-normal PDFs for the engine point at 4500 RPM WOT.

PMAX Model

The maximum in-cylinder pressure is one of the main inputs of the knock model discussed above. The method developed by the authors in [26] for the PMAX estimation is introduced within the engine simulator. As demonstrated in [26], PMAX can be modelled with a polynomial equation with the engine load (defined as the trapped air mass per cycle, per cylinder) and the CA50 as independent variables. This method is robust because it allows to reproduce the PMAX with a simple mathematical formulation and a high level of accuracy even for experimental setups with Port Water Injection or Low-Pressure Exhaust Gas Recirculation systems [26]. In Figure 12 the polynomial equation (the surface) and the mean experimental PMAX values (red dots) are shown. The accuracy of such approach is further demonstrated because the RMSE between the experimental and the calculated points is equal to 2.21 bar. The CA50 values reported in Figure 12 are scaled with respect to the minimum value of the dataset, for confidential reasons. Thus, the units reported in the left-hand graph are ΔCA50. Such method is applied to all the figures that include CA50.

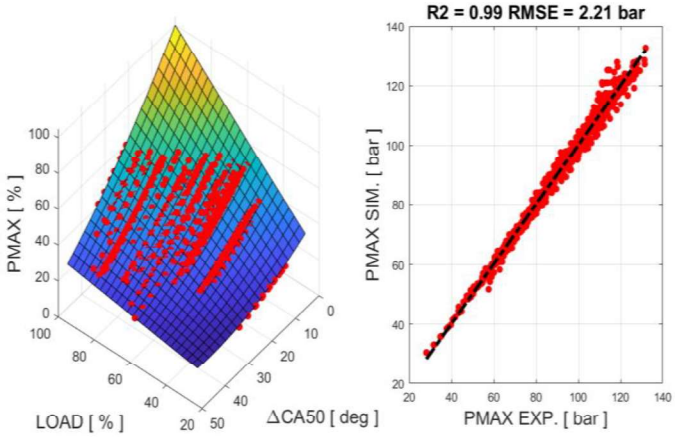

Figure 12. Polynomial function and experimental PMAX values on the CA50-load domain (left-hand graph) and the regression analysis of the experimental and the calculated PMAX.

Exhaust Gas Temperature model

One of the novel contributions of this work with respect to [8] is the definition of the exhaust gas temperature sensitivity to the lambda value. The 0-D combustion model determines the in-cylinder pressure curve including the effect of lambda. This means that it is possible to calculate TEVO for the entire engine operating field. In Figure 13 the simulated TEVO is reported for three different lambda values on the CA50 domain, for 4500 RPM and WOT operating conditions.

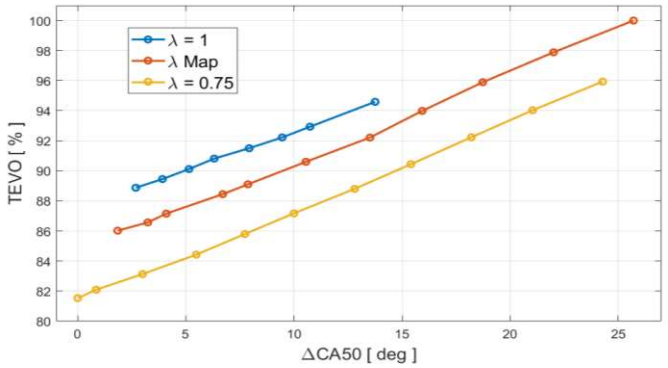

Figure 13. Trends of the TEVO for some spark sweeps carried out at 4500 RPM WOT with different lambda values.

The Figure 13 shows that the TEVO can be modelled with a first-degree polynomial function with the CA50 as independent variable. Moreover, the angular coefficient of such linear function can be fixed for different lambda values. The TEVO variation due to different lambda value can be accurately described with a first order polynomial, once the engine speed, load and CA50 are fixed. In Figure 14 such trend is shown for three different values of CA50 at 4500 RPM and WOT.

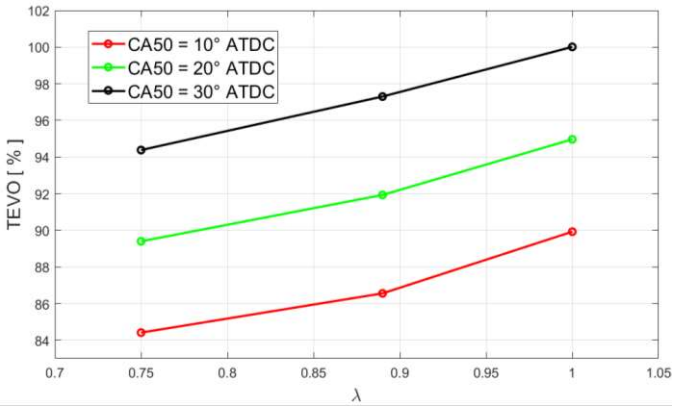

Figure 14. TEVO simulated at 4500 RPM WOT for different lambda and CA50 values.

Three different polynomials are developed for three lambda values (0.75, the value of the standard map, and 1). All these equations have the same analytical formulation shown below:

$$TEVO = A_{TEVO}\ CA50 + B_{TEVO} \tag{13}$$

$$A_{TEVO} = a_{00} + a_{10}X + a_{01}Y + a_{20}X^2 + a_{11}XY + a_{02}Y^2 + a_{21}X^2Y + a_{12}XY^2 + a_{03}Y^3 \tag{14}$$

$$B_{TEVO} = b_{00} + b_{10}X + b_{01}Y + b_{20}X^2 + b_{11}XY + b_{02}Y^2 + b_{21}X^2Y + b_{12}XY^2 + b_{03}Y^3 \tag{15}$$

Where X and Y represent the engine speed and load, respectively. The coefficients of the equations (14) and (15) are calibrated by minimizing the R2 index estimated between the polynomial and the punctual values. The polynomial degree is chosen as the lowest value that provides a significant increase of the R2 (i.e., 10^{-2}), to have a simple formulation and to avoid the overfitting phenomenon. The TEVO is thus calculated for the three reference lambda values, for fixed engine load, speed and CA50, and the value that corresponds to the current lambda is determined by fitting these three temperatures. The resulting scheme of such model is shown in Figure 15.

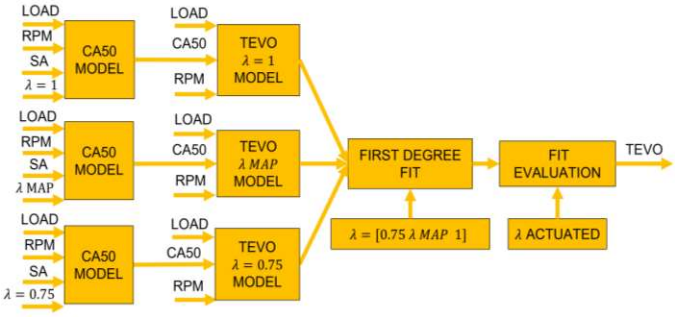

Figure 15. Complete scheme of the TEVO model

The simulated TEVO is then converted into the temperature recorded within the exhaust pipes through the polynomial function introduced in [8]. Figure 16 shows the difference between the TEVO, and the mean experimental exhaust gas temperature measured at the turbine inlet (ΔT) for different operating conditions.

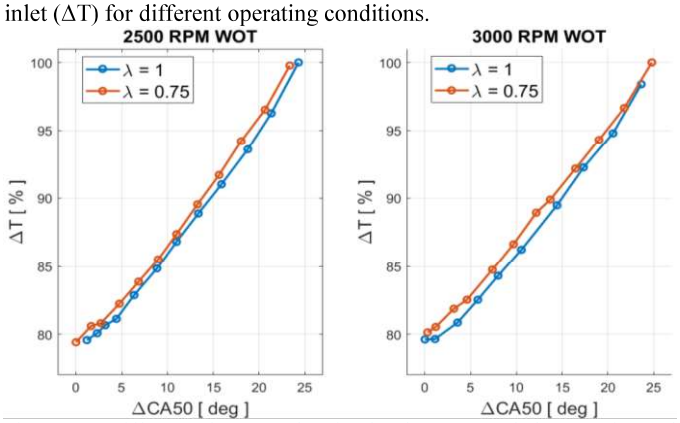

Figure 16. Difference between the simulated TEVO and the experimental exhaust gas temperature at turbine inlet (ΔT) at 2500 RPM WOT and 3000 RPM WOT, with rich and stoichiometric mixture.

Such result shows that the difference between the trends related to the stochiometric and the rich mixtures is under the 1.5 % and this means that such gap can be neglected without introducing a significant accuracy loss. Therefore, as shown in Figure 16, the ΔT can be described with a first order polynomial with the CA50 as independent variable. The analytical formulation of such corrective function, introduced in [8], is still accurate even for this experimental setup. Figure 17 shows the block scheme of the mentioned function.

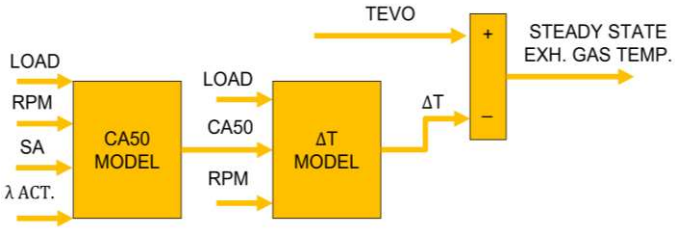

Figure 17. Scheme of the function used to calculate the exhaust gas temperature at the turbine inlet.

The accuracy of the resulting approach for the exhaust gas temperature calculation is demonstrated by comparing the calculated and the experimental values for the whole available dataset. As shown in Figure 18, the R2 and the RMSE between the experimental and the simulated values is about 0.97 and 12 C°, respectively. Considering that for the standard type K, 3 mm thermocouple the uncertainty on the measurement due to the radiation, conduction, and the finite mass of the sensor is about 40 °C [36], the accuracy of the proposed model is further demonstrated (the calculated RMSE is four times lower than such uncertainty).

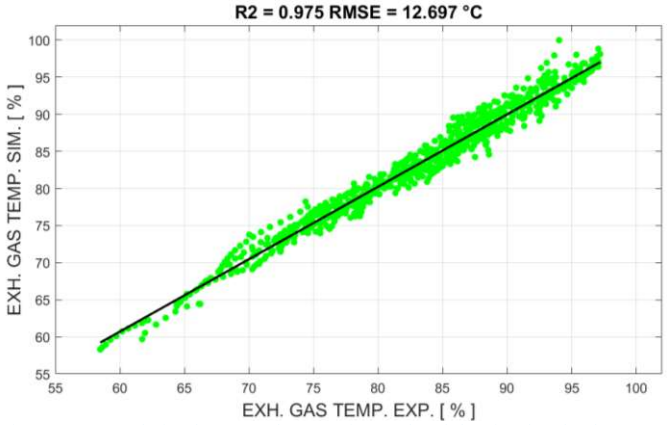

Figure 18. Correlation between the experimental and the simulated exhaust gas temperature.

The percentage error between the calculated and the experimental values is included within the range ±6%, with a standard deviation of 1.5 %. The Figure 19 shows the histogram and the Gaussian Statistical distribution of such data.

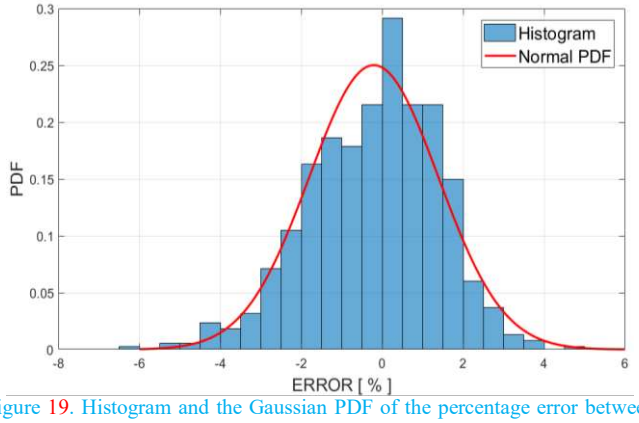

Figure 19. Histogram and the Gaussian PDF of the percentage error between the experimental and the simulated exhaust gas temperature.

Target Lambda Map Calibration

A Design of Experiment (DoE) method is applied to calculate the values of the target lambda and the SA to maximize the combustion efficiency on the entire engine operating field, using the virtual engine developed above. The KLSA is determined with a FEM-based, piston damage model described by the authors in [30]. In this way, the knock intensity is evaluated through a concrete and a tangible index, and this allows to increase the combustion efficiency. The admissible intensity of knocking events is completely redefined and the KLSA is determined as the spark timing that ensures the target piston damage speed.

Coupling the engine simulator with the piston damage model, the algorithm shown in Figure 20 is implemented to calibrate the target lambda map. The main steps of the proposed iterative procedure are the following:

1. For fixed load, speed and lambda, the CA50 is calculated starting from a retarded SA value with respect to the mapped one
2. Exploiting the simulated CA50, the correspondent values of PMAX and the exhaust gas temperature are calculated.
3. Using a constant value of 35 C° for the intake air temperature, the knock model generates cyclic MAPO values in accordance with the calculated PDF parameters.
4. Taking as inputs the cyclic MAPO values, PMAX and RPM the piston damage model calculates the damage speed that is compared with the target value.
5. Such iterative algorithm proceeds increasing the SA until the simulated damage speed is higher than the target. With such method the trend of the exhaust gas temperature is obtained as a function of the SA, for fixed values of the engine load, speed, and lambda. Figure 20 shows this trend for the engine point at 7500 RPM and WOT. The exhaust gas temperature value that corresponds to the admissible damage speed is highlighted.
6. The procedure described from point 1 to 5 is repeated for different values of lambda and in this way the trend of the exhaust gas temperature (for the KLSA) is determined as a function of lambda, for each engine point. Figure 22 shows this curve, and it is superposed to the maximum exhaust gas temperature defined by the turbocharger manufacturer. The lambda value that corresponds to this maximum temperature is defined as the target value for the given engine operating condition. Such algorithm reduces the specific fuel consumption and guarantees the turbine impeller integrity.

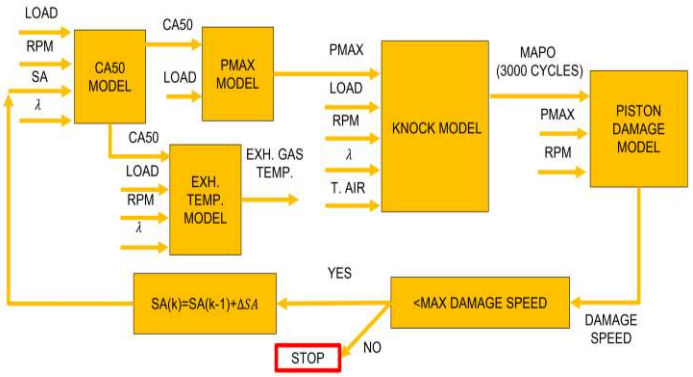

Figure 20. Iterative loop applied to identify the KLSA for each engine operating conditions.

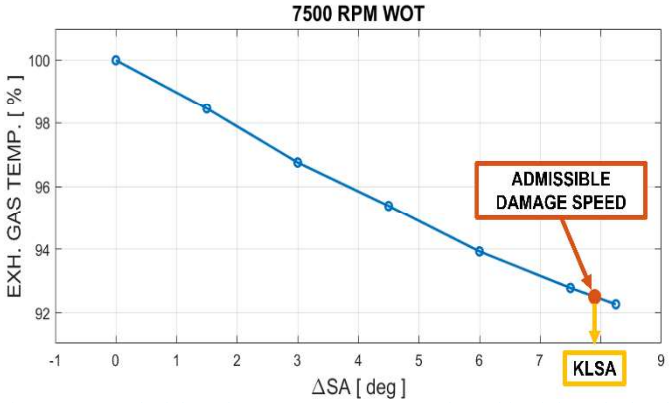

Figure 21. Trend of the exhaust gas temperature at the turbine inlet calculated with the iterative loop shown in Figure 20. For confidentiality reasons, the SA values are scaled with respect to the minimum value reported on the x-axis.

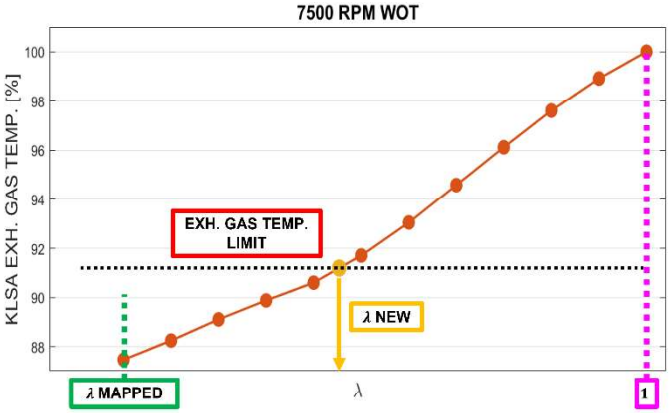

Figure 22. Trend of the exhaust gas temperature for the KLSA as a function of lambda.

The described procedure allows to extend the stoichiometric area of the engine operating field of 18 %, with respect to the standard lambda map. Such value is determined as the ratio between the number of the engine points (i.e., the breakpoints of the ECU maps) with a target lambda equal to 1 for the recalibrated and the production maps.

Experimental Validation

The results of the experimental tests performed with the lambda map calibrated with the algorithm presented above are shown in this section. Such tests are carried out by managing the SA with the piston damage-based, combustion control system described by the authors in [30] and [31]. In this way, the SA is controlled to get the target piston damage speed under knock-limited operating conditions, even during real on-vehicle maneuvers.
The engine is operated by reproducing a speed and a pedal profile recorded during a fixed-gear, vehicle acceleration. In Figure 23 the pedal, the speed and the load (always reported as the normalized trapped air mass, per cycle, per cylinder) traces of the experimental tests are shown.

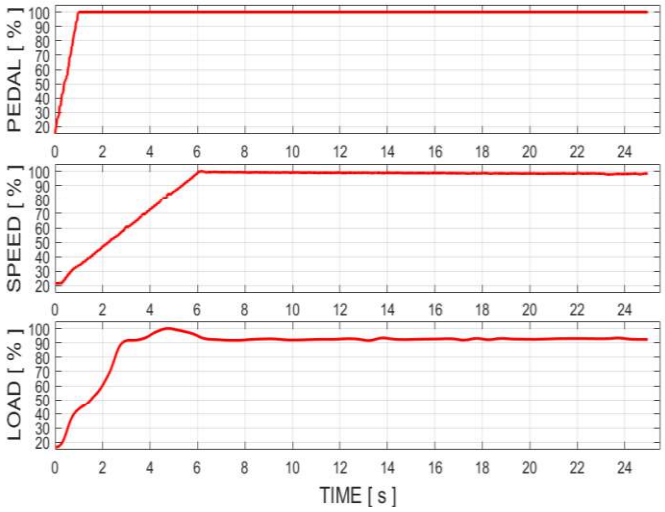

Figure 23. Pedal, engine speed and load traces of the experimental tests.

It is important to mention that after a few seconds the vehicle maneuver is concluded. Nevertheless, the engine speed and load are kept constant for several seconds. This is useful to reach the steady state condition of the thermocouple measurement, that is affected by a slow response under transient conditions. In this way it is possible to perform a robust comparison between the exhaust gas temperature profiles measured on different tests, for both the transient and the steady-state conditions. Indeed, the traces reported in Figure 23 are repeated for three times. The first test is carried out with the stock SA and lambda maps (named test 1 in the following graphs) and it represents the reference condition. The second test is performed with the SA calculated by the piston damage-based controller and the standard lambda map (test 2). The third test is carried out with the SA controller, and the lambda map optimized with the model-based procedure described above (test 3). In Figure 24 the exhaust gas temperature measured at the turbine inlet during such tests is shown in the graph on top, while the temperature difference between the test 2 and 1, and between the tests 3 and 1 are reported in the second graph from top. The two bottom graphs show the CA50, and the lambda profiles measured during the experimental tests, respectively, and the latter is reported without the y-axis scale for confidentiality reasons.

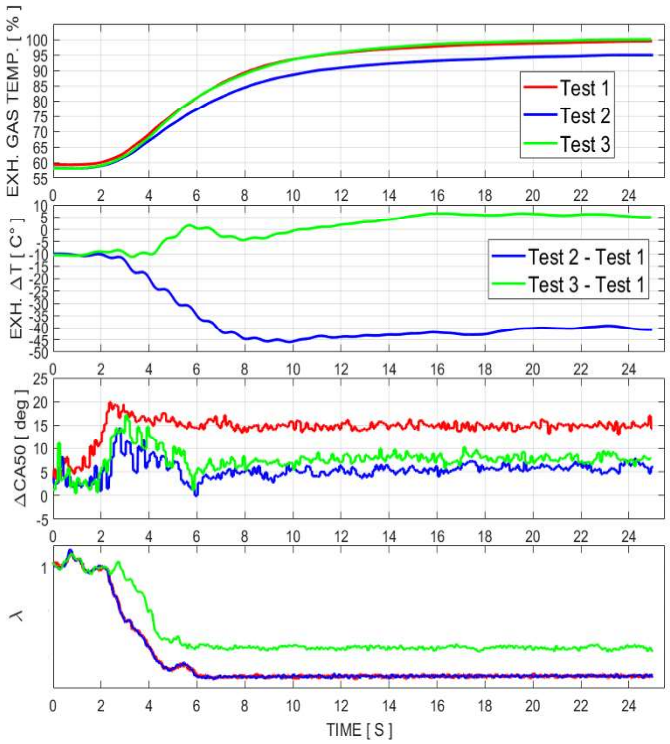

Figure 24. The measured exhaust gas temperature profiles at the turbine inlet (graph on top), the temperature difference between the test 2 and 1, and between the test 3 and test 1 (second graph from top), the filtered CA50 (third graph from top) and lambda, measured under transient conditions.

Analyzing the first subplot of Figure 24, the red line represents the exhaust gas temperature measured at the turbine inlet recorded with the standard SA and lambda maps. Operating the engine for reaching the target piston damage speed and with the standard lambda map, it is possible to increase the combustion efficiency with respect to the standard SA map, reducing the exhaust gas temperature of 45 °C (Figure 24, second graph from top). Such temperature reduction achieved with the same target lambda of the test 1 demonstrates that the turbine impeller works under its maximum temperature limit. For this reason, it is possible to decrease the mixture enrichment, reobtaining the maximum exhaust gas temperature (i.e., the reference value recorded during the test 1). In other words, the aim is that to have the green and the red lines superposed. This objective is achieved because the maximum difference between the inlet turbine gas temperature for the test 1 and 3 is close to 5 C°, under high engine load and speed operating conditions (this means that the difference is lower than 1% between the two tests). It can be stated that the combustion controller actuates a retarded spark advance during the test 3, with respect to the test 2. This is because the knock tendency increases by reducing the mixture enrichment, and the piston damage-based controller can evaluate the SA that allows to keep constant the piston erosion speed.
Finally, it is possible to state that the model-based procedure for the lambda map calibration is particularly reliable because the gained combustion efficiency is converted into a higher lambda value, targeting the maximum exhaust gas temperature (recorded during the test 1) with high accuracy.
The overall efficiency increase achieved during the test 2 and 3 with respect to the test 1 is finally evaluated. Such analysis is carried out considering the specific fuel consumption. Figure 25 shows the efficiency increase achieved with the test 2 with respect to the reference (test 1). The black dots represent the engine points touched during the experimental tests and they are reported on the speed-load field.

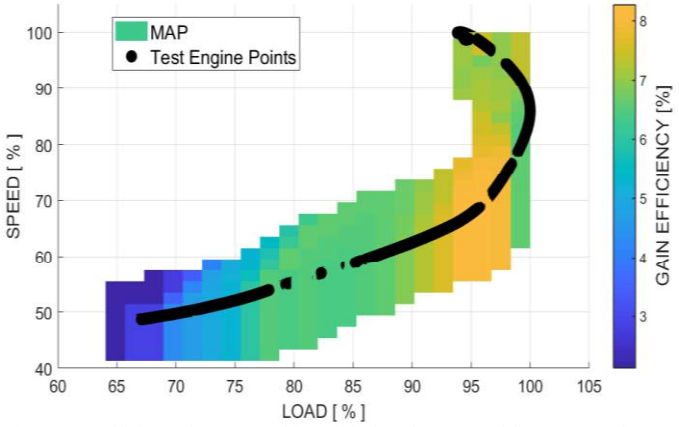

Figure 25. Efficiency increase achieved during the test 2 with respect to the test 1. The red dots represent the engine points touched during the experimental tests.

Figure 26 shows the same analysis of Figure 25 for the test 3.

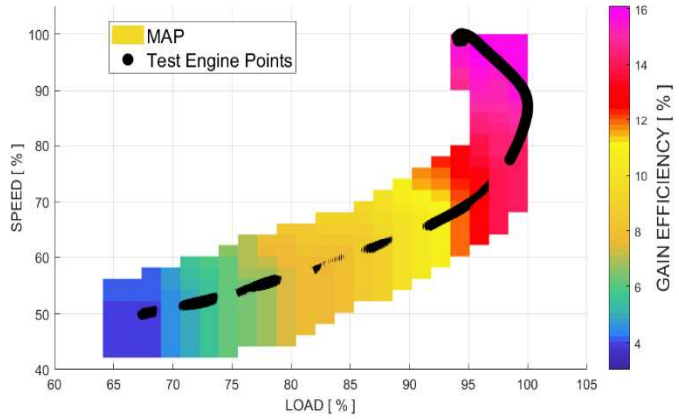

Figure 26. Efficiency increase achieved during the test 3 with respect to the test 1. The red dots represent the engine points touched during the experimental tests.

The values shown in Figures 25 and 26 can be considered as a remarkable result. Indeed, managing the combustion phase with the innovative piston damage-based controller, it is possible to increase the overall engine efficiency of about 8 %, especially under high engine speed and load operating conditions. Indeed, these are the engine points for which knock, and the exhaust gas temperatures represent the main causes of the efficiency loss. Finally, introducing even the lambda map calibrated with the innovative, model-based algorithm described in this work, a reduction of about 16 % of the specific fuel consumption is achieved.

Conclusions and Future Works

In this work, the authors propose a novel methodology to automatically calibrate the lambda map, managing the SA with an innovative piston damage-based combustion controller [30, 31]. The CA50 and the exhaust gas temperature models are improved with respect previous works [8] by introducing the sensitivity to the lambda value. A single layer FNN is used to calculate the combustion phase receiving the SA, engine load, speed, and lambda as inputs. Such modeling approach guarantees a high accuracy (0.63 CA° of RMSE on the testing dataset) and a low execution time. On the other hand, the introduction of the lambda sensitivity in the exhaust gas temperature model is carried out maintaining a formulation similar to the one described in [8]. The accuracy of the model is analyzed and the Gaussian PDF of the error between the experimental and the simulated values is presented. It is characterized by a standard deviation of 1.5 % and thus the 95 % of the simulated values are calculated with an error included within the range of $\pm$ 3 %. The KLSA is calculated with a DoE for each engine operating condition. Coupling the function for estimating the exhaust gas temperature with the piston damage model [30], the SA value that allows to target the admissible piston damage speed is determined. The procedure is repeated for different lambda values and the curve of the exhaust gas temperatures that corresponds to the KLSA is defined as a function of lambda. Finding the interpolation between such curve and the maximum temperature of the exhaust gasses (determined by the turbine manufacturer), the lambda map is calibrated to minimize the specific fuel consumption.

In the last part of this work such calibrated values are validated through experimental tests. A piston damage-based combustion controller is applied to manage the SA for targeting the admissible piston damage speed. The experimental tests are carried out reproducing at the engine test bench a pedal and an engine speed profile recorded during a real, fixed-gear, vehicle acceleration. An overall efficiency increase of about 7% can be reached due to the innovative management of knock intensity (and thus of the SA) with the standard lambda map, while an improvement of 16% is achieved by applying the calibrated lambda map.

In this work, the same type of gasoline is used to collect the database for both the algorithm development and validation. The discussed model-based procedure for the lambda map calibration does not consider the fuel RON. As well known, using a different type of gasoline, the lambda value needed to reach the same exhaust gas temperature changes. This because of a different combustion phase reached to target the admissible piston damage speed. For this reason, further improvement will be applied to the FNN-based models to include the sensitivity to the fuel RON. Moreover, the exhaust gas temperature model will be directly introduced within the piston damage-based combustion controller, to actively calculate and control the target lambda value needed to reduce the specific fuel consumption and to prevent the turbine failure. Indeed, the pure analytical formulation of this function allows to easily reverse the equations, converting it into a control algorithm.

References

1. Cavina, N., Mancini, G., Corti, E., Moro, D. et al., "Thermal Management Strategies for SCR After Treatment Systems," SAE Technical Paper 2013-24-0153, 2013, https://doi.org/10.4271/2013-24-0153.
2. Zhao, F., "Technologies for Near-Zero-Emission Gasoline-Powered Vehicles", SAE International, 2006, Warrendale, USA, ISBN13: 9780768014617
3. Gainey, B., Gohn, J., Yan, Z., Malik, K. et al., "HCCI with Wet Ethanol: Investigating the Charge Cooling Effect of a High Latent Heat of Vaporization Fuel in LTC," SAE Technical Paper 2019-24-0024, 2019, https://doi:10.4271/2019-24-0024.
4. Szybist, J., Wagnon, S., Splitter, D., Pitz, W. et al., "The Reduced Effectiveness of EGR to Mitigate Knock at High Loads in Boosted SI Engines," *SAE Int. J. Engines* 10(5):2305-2318, 2017, https://doi.org/10.4271/2017-24-0061.
5. Cavina, N., Rojo, N., Businaro, A., Brusa, A. et al., "Investigation of Water Injection Effects on Combustion Characteristics of a GDI TC Engine," *SAE Int. J. Engines* 10(4):2017, https://doi:10.4271/2017-24-0052.
6. Stadler, A., Sauerland, H., Härtl, M., and Wachtmeister, G., "The Potential of Gasoline Fueled Pre Chamber Ignition Combined with Elevated Compression Ratio," SAE Technical Paper 2020-01-0279, 2020, https://doi:10.4271/2020-01-0279.
7. Tricker, D., Egger, A., Krus, D., and Bredda, S., "Impact of High-Performance Combustion Chamber Alloys on Fuel Efficiency," SAE Int. J. Advances & Curr. Prac. in Mobility 2(5):2918-2924, 2020, https://doi:10.4271/2020-01-1338.
8. Brusa, A., Cavina, N., Rojo, N., Cucchi, M. et al., "Development and Validation of a Control-Oriented Analytic Engine

Simulator," SAE Technical Paper 2019-24-0002, 2019, https://doi.org/10.4271/2019-24-0002.
9. Wang, S., Prucka, R., Zhu, Q., Prucka, M. et al., "A Real-Time Model for Spark Ignition Engine Combustion Phasing Prediction," *SAE Int. J. Engines* 9(2):2016, https://doi:10.4271/2016-01-0819.
10. Bidarvatan, M., Shahbakhti, M. and Jazayeri, S., "Model-Based Control of Combustion Phasing in an HCCI Engine," *SAE Int. J. Engines* 5(3):2012, https://doi:10.4271/2012-01-1137.
11. Johnson, R., Kaczynski, D., Zeng, W., Warey, A. et al., "Prediction of Combustion Phasing Using Deep Convolutional Neural Networks," SAE Technical Paper 2020-01-0292, 2020, https://doi:10.4271/2020-01-0292.
12. Wunderlin S., Hurstel A., Kloppenburg E. (2017) "Implementing a real time exhaust gas temperature model for a Diesel engine with ASC@ECU". In: Bargende M., Reuss HC., Wiedemann J. (eds) 17. Internationales Stuttgarter Symposium. Proceedings. Springer Vieweg, Wiesbaden. https://doi.org/10.1007/978-3-658-16988-6_79
13. Coraddu, A., Oneto, L., Cipollini, F., Kalikatzarakis, M., Meijn, G. J., & Geertsma, R. (2021). "Physical, datadriven and hybrid approaches to model engine exhaust gas temperatures in operational conditions". Ships and Offshore Structures. https://doi.org/10.1080/17445302.2021.1920095
14. A. Kumar, A. Srivastava, N. Goel and J. McMaster, "Exhaust gas temperature data prediction by autoregressive models," 2015 IEEE 28th Canadian Conference on Electrical and Computer Engineering (CCECE), 2015, pp. 976-981, doi: 10.1109/CCECE.2015.7129408.
15. Hajireza, S., Mauss, F., Sunden, B., "Two-Zone Model of Gas Thermodynamic State in SI Engines with Relevance for Knock," presented at the international symposium on diagnostics and modeling of combustion in internal combustion engines COMODIA90, Japan, September 3-5, 1990.
16. Moses, E., Yarin, A.L., and Bar-Yoseph, P. "On knocking prediction in spark ignition engines," Combustion and Flame 101(3): 239-261, 1995, https://doi:10.1016/0010-2180(94)00202-4.
17. Kozarac, D., Tomic, R., Taritas, I., Chen, J. et al., "A Model for Prediction of Knock in the Cycle Simulation by Detail Characterization of Fuel and Temperature Stratification," *SAE Int. J. Engines* 8(4):2015, https://doi:10.4271/2015-01-1245.
18. Livengood, J.C., Wu, P.C., "Correlation of Auto-ignition Phenomena in Internal Combustion Engines and Rapid Compression Machines," Symposium (International) on Combustion 5(1): 347-356, 1955, https://doi:10.1016/S0082-0784(55)80047-1.
19. Khan, A., Burluka, A., Neumeister, J., OudeNijeweme, D. et al., "Combustion and Autoignition Modelling in a Turbocharged SI Engine," *SAE Int. J. Engines* 9(4):2016, https://doi:10.4271/2016-01-2234.
20. Bozza, F., De Bellis, V., Minarelli, F., and Cacciatore, D., "Knock and Cycle by Cycle Analysis of a High Performance V12 Spark Ignition Engine. Part 2: 1D Combustion and Knock Modeling," *SAE Int. J. Engines* 8(5):2015, https://doi:10.4271/2015-24-2393.
21. Corti, E., Forte, C., Bianchi, G., and Zoffoli, L., "A Control-Oriented Knock Intensity Estimator," *SAE Int. J. Engines* 10(4):2017, https://doi:10.4271/2017-24-0055.
22. Ghandhi, J. and Kim, K., "A Statistical Description of Knock Intensity and Its Prediction," SAE Technical Paper 2017-01-0659, 2017, https://doi:10.4271/2017-01-0659.
23. Yang, Z., Rao, S., Wang, Y., Harsulkar, J. et al., "Investigation of Combustion Knock Distribution in a Boosted Methane-Gasoline Blended Fueled SI Engine," SAE Technical Paper 2018-01-0215, 2018, https://doi:10.4271/2018-01-0215.
24. Cavina, N., Brusa, A., Rojo, N., and Corti, E., "Statistical Analysis of Knock Intensity Probability Distribution and Development of 0-D Predictive Knock Model for a SI TC Engine," SAE Technical Paper2018-01-0858, 2018, https://doi:10.4271/2018-01-0858.
25. Mecagni, J., Brusa, A.,Cavina, N., Corti, E. et al.,"Control-Oriented Exhaust Gas Temperature Modelling Based on Wiebe Equation," *SAE Int. J. Engines* 14(5):2021, https://doi:10.4271/03-14-05-0042.
26. Scocozza, G., Silvagni, G., Brusa, A., Cavina, N. et al., "Development and Validation of a Virtual Sensor for Estimating the Maximum in-Cylinder Pressure of SI and GCI Engines," SAE Technical Paper 2021-24-0026, 2021, https://doi.org/10.4271/2021-24-0026.
27. Spelina, J., Peyton Jones, J., and Frey, J., "Recent Advances in Knock Analysis, Simulation, and Control," SAE Int. J. Engines 7(2):2014, https://doi:10.4271/2014-01-1349.
28. Peyton Jones, J. and Frey, J., "Threshold Optimization and Performance Evaluation of a Classical Knock Controller," *SAE Int. J. Engines* 8(3):2015, https://doi:10.4271/2015-01-0871.
29. Cavina, N., Rojo, N., Ceschini, L., Balducci, E. et al., "Investigation of Knock Damage Mechanisms on a GDI TC Engine," SAE Technical Paper 2017-24-0060, 2017, https://doi.org/10.4271/2017-24-0060.
30. Brusa, A.; Cavina, N.; Rojo, N.; Mecagni, J.; Corti, E.; Ravaglioli, V.; Cucchi, M.; Silvestri, N. Development and Experimental Validation of an Adaptive, Piston-Damage-Based Combustion Control System for SI Engines: Part 1—Evaluating Open-Loop Chain Performance. Energies 2021, 14, 5367. https://doi.org/10.3390/en14175367
31. Brusa, A.; Cavina, N.; Rojo, N.; Mecagni, J.; Corti, E.; Moro, D.; Cucchi, M.; Silvestri, N. Development and Experimental Validation of an Adaptive, Piston- Damage- Based Combustion Control System for SI Engines: Part 2–Implementation of Adaptive Strategies. *Energies* 2021, *14*, 5342. https://doi.org/10.3390/en14175342
32. Loganathan, S., Murali Manohar, R., Thamaraikannan, R., Dhanasekaran, R. et al., "Direct Injection Diesel Engine Rate of Heat Release Prediction using Universal Load Correction Factor in Double Wiebe Function for Performance Simulation," SAE Technical Paper 2011-01-2456, 2012, https://doi.org/10.4271/2011-01-2456.
33. Matlab Documentation, The MathWorks, 2020, https://www.mathworks.com/.
34. Møller, Martin Fodslette. "A scaled conjugate gradient algorithm for fast supervised learning." Neural Networks 6 (1993): 525-533, https://doi:10.1016/S0893-6080(05)80056-5.
35. Hoth, A., Pulpeiro Gonzalez, J., Kolodziej, C., and Rockstroh, T., "Effects of Lambda on Knocking Characteristics and RON Rating," *SAE Int. J. Adv. & Curr. Prac. in Mobility* 1(3):1188-1201, 2019, https://doi-org.ezproxy.unibo.it/10.4271/2019-01-0627.
36. Papaioannou, N., Leach, F., and Davy, M. (June 30, 2020). "Improving the Uncertainty of Exhaust Gas Temperature Measurements in Internal Combustion Engines." ASME. *J. Eng. Gas Turbines Power*. July 2020; 142(7): 071007. https://doi.org/10.1115/1.4047283

Definitions/Abbreviations

ANN	Artificial Neural Network
ATDC	After Top Dead Center
BTDC	Before Top Dead Center
CA	Crank Angle

CA50	Crank Angle correspondent to 50% of Mass Fuel Burnt
DoE	Design of Experiment
ECU	Engine Control Unit
FEM	Finite Element Method
FNN	Feedforward Neural Network
GDI	Gasoline Direct Injection
KLSA	Knock Limited Spark Advance
MAPO	Maximum Amplitude of Pressure Oscillation
PDF	Probability Density Function
R2	R-Square
RMSE	Root Mean Square Error
RON	Research Octane Number
RT	Real Time
SI	Spark Ignition
SOC	Start of Combustion
TC	Turbo-Charged
TEVO	Temperature at Exhaust Valve Opening
WOT	Wide Open Throttle